

## The PAMELA Space Mission for Antimatter and Dark Matter Searches in Cosmic Rays

O. Adriani, G. C. Barbarino, G. A. Bazilevskaia, R. Bellotti, M. Boezio et al.

Citation: *AIP Conf. Proc.* **1223**, 33 (2010); doi: 10.1063/1.3395994

View online: <http://dx.doi.org/10.1063/1.3395994>

View Table of Contents: <http://proceedings.aip.org/dbt/dbt.jsp?KEY=APCPCS&Volume=1223&Issue=1>

Published by the [American Institute of Physics](#).

---

### Related Articles

A mathematical theory of stochastic microlensing. I. Random time delay functions and lensing maps  
*J. Math. Phys.* **50**, 072503 (2009)

From Dirac spinor fields to eigenspinoren des Ladungskonjugationsoperators  
*J. Math. Phys.* **48**, 123517 (2007)

Enhanced ballistic phonon production for surface events in cryogenic silicon detector  
*Appl. Phys. Lett.* **76**, 2958 (2000)

A simultaneous solution to baryogenesis and dark-matter problems  
*Phys. Part. Nucl.* **29**, 257 (1998)

Ionimplanted charge collection contacts for high purity silicon detectors operated at 20 mK  
*Rev. Sci. Instrum.* **66**, 2625 (1995)

---

### Additional information on AIP Conf. Proc.

Journal Homepage: <http://proceedings.aip.org/>

Journal Information: [http://proceedings.aip.org/about/about\\_the\\_proceedings](http://proceedings.aip.org/about/about_the_proceedings)

Top downloads: [http://proceedings.aip.org/dbt/most\\_downloaded.jsp?KEY=APCPCS](http://proceedings.aip.org/dbt/most_downloaded.jsp?KEY=APCPCS)

Information for Authors: [http://proceedings.aip.org/authors/information\\_for\\_authors](http://proceedings.aip.org/authors/information_for_authors)

### ADVERTISEMENT



**AIP**Advances

*Submit Now*

**Explore AIP's new  
open-access journal**

- **Article-level metrics  
now available**
- **Join the conversation!  
Rate & comment on articles**

# The PAMELA Space Mission for Antimatter and Dark Matter Searches in Cosmic Rays

O. Adriani<sup>\*</sup>, G. C. Barbarino<sup>†</sup>, G. A. Bazilevskaja<sup>\*\*</sup>, R. Bellotti<sup>‡</sup>,  
M. Boezio<sup>§</sup>, E. A. Bogomolov<sup>¶</sup>, L. Bonechi<sup>\*</sup>, M. Bongi<sup>\*</sup>, V. Bonvicini<sup>§</sup>,  
S. Borisov<sup>||</sup>, S. Bottai<sup>\*</sup>, A. Bruno<sup>‡</sup>, F. Cafagna<sup>‡</sup>, D. Campana<sup>†</sup>,  
R. Carbone<sup>†</sup>, P. Carlson<sup>††</sup>, M. Casolino<sup>||</sup>, G. Castellini<sup>‡‡</sup>, L. Consiglio<sup>†</sup>,  
M. P. De Pascale<sup>||</sup>, C. De Santis<sup>||</sup>, N. De Simone<sup>||</sup>, V. Di Felice<sup>||</sup>,  
A. M. Galper<sup>§§</sup>, W. Gillard<sup>††</sup>, P. Hofverberg<sup>††</sup>, S. V. Koldashov<sup>§§</sup>,  
S. Y. Krutkov<sup>¶</sup>, A. N. Kvashnin<sup>\*\*</sup>, A. Leonov<sup>§§</sup>, V. Malvezzi<sup>||</sup>,  
L. Marcelli<sup>||</sup>, W. Menn<sup>¶¶</sup>, V. V. Mikhailov<sup>§§</sup>, E. Mocchiutti<sup>§</sup>, N. Mori<sup>\*</sup>,  
N. N. Nikonov<sup>¶</sup>, G. Osteria<sup>†</sup>, P. Papini<sup>\*</sup>, M. Pearce<sup>††</sup>, P. Picozza<sup>||</sup>,  
M. Ricci<sup>\*\*\*</sup>, S. B. Ricciarini<sup>\*</sup>, M. Simon<sup>¶¶</sup>, R. Sparvoli<sup>||</sup>, P. Spillantini<sup>\*</sup>,  
Y. I. Stozhkov<sup>\*\*</sup>, A. Vacchi<sup>§</sup>, E. Vannuccini<sup>\*</sup>, G. Vasilyev<sup>¶</sup>,  
S. A. Voronov<sup>§§</sup>, Y. T. Yurkin<sup>§§</sup>, G. Zampa<sup>§</sup>, N. Zampa<sup>§</sup> and V. G. Zverev<sup>§§</sup>

<sup>\*</sup>INFN, Structure of Florence and Physics Department of University of Florence, Via Sansone 1,  
I-50019 Sesto Fiorentino, Florence, Italy

<sup>†</sup>INFN, Structure of Naples and Physics Department of University of Naples Federico II, Via  
Cintia, I-80126 Naples, Italy

<sup>\*\*</sup>Lebedev Physical Institute, Leninsky Prospekt 53, RU-119991 Moscow, Russia

<sup>‡</sup>INFN, Structure of Bari and Physics Department of University of Bari, Via Amendola 173,  
I-70126 Bari, Italy

<sup>§</sup>INFN, Structure of Trieste, Padriciano 99, I-34012 Trieste, Italy

<sup>¶</sup>IOFFE Physical Technical Institute, Polytekhnicheskaya 26, RU-194021 St. Petersburg, Russia

<sup>||</sup>INFN, Structure of Rome Tor Vergata and Physics Department of University of Rome Tor Vergata,  
Via della Ricerca Scientifica 1, I-00133 Rome, Italy

<sup>††</sup>KTH Department of Physics, Albanova University Centre, SE-10691 Stockholm, Sweden

<sup>‡‡</sup>IFAC, Via Madonna del Piano 10, I-50019 Sesto Fiorentino, Florence, Italy

<sup>§§</sup>Moscow Engineering and Physics Institute, Kashirskoe Shosse 31, RU-11540 Moscow, Russia

<sup>¶¶</sup>Universitat Siegen, D-57068 Siegen, Germany

<sup>\*\*\*</sup>INFN, Laboratori Nazionali di Frascati, Via Enrico Fermi 40, I-00044 Frascati, Italy

**Abstract.** On the 15<sup>th</sup> of June 2006, the PAMELA satellite-borne experiment was launched from the Baikonur cosmodrome and it has been collecting data since July 2006. The instrument allows precision studies of the charged cosmic radiation to be conducted over a wide energy range (100 MeV - 100's GeV) with high statistics. The primary scientific goal is the measurement of the antiproton and positron energy spectrum in order to search for exotic sources, such as dark matter particle annihilations. PAMELA is also searching for primordial antinuclei (anti-helium), and testing cosmic-ray propagation models through precise measurements of the antiparticle energy spectrum and precision studies of light nuclei and their isotopes. Moreover, PAMELA is investigating phenomena connected with solar and earth physics. Results of the antiproton and positron data will be presented.

## INTRODUCTION

PAMELA is a satellite born particle spectrometer. It has been designed to measure in detail the spectra of primary and secondary components of the cosmic radiation. Its major scientific goal is the precise measurement of antiprotons and positrons spectra in cosmic rays, over the largest energy range ever achieved. The precise knowledge of these spectra behaviour, especially in the energy range larger than 50 GeV, can lead to the indirect detection of dark matter. Its design lifetime is more than three year of data taking, providing unprecedented statistics with no atmospheric overburden reducing the systematic uncertainties of previous measurements obtained mainly by balloon-borne experiments.

PAMELA is housed inside a pressurized container attached to the Russian satellite Resurs-DK1. It was launched into space on the 15<sup>th</sup> June 2006, by a Soyuz-U rocket, from the Baikonur cosmodrome in Kazakhstan, and deployed in a semi-polar (70°) elliptical orbit at an altitude in the range 350–600 km. PAMELA was switched on for the first time on 21<sup>st</sup> June 2006 and has been in a nearly continuous data taking since 11<sup>th</sup> July 2006.

## PAMELA APPARATUS

The PAMELA apparatus is composed of the following sub-detectors stacked, as in Fig. 1, from top to bottom: a time of flight system (ToF) (S1,S2,S3), a magnetic spectrometer, an anticoincidence system (CARD, CAT, CAS), an electromagnetic imaging calorimeter, a shower tail catcher scintillator (S4), and a neutron detector [1].

The ToF is made of 3 double-layer of plastic scintillator paddles. It provides the first-level trigger and helps in particle identification, for rigidities(R) lower than 1GV, and in rejecting albedo particles by measuring particle  $\beta$  and  $dE/dx$ .

Particle rigidity and charge sign are determined by the silicon spectrometer. Six layer of double-side silicon sensors are stacked in between five permanent magnet modules. Thanks to spatial resolution of  $3\div 4\ \mu\text{m}$  and  $8\div 13\ \mu\text{m}$ , in bending and not bending view respectively, it is possible to reach a maximum detectable rigidity (MDR) of  $\approx 1\ \text{TeV}/c$ .

A plastic scintillator anticoincidence system shields the spectrometer, covering the magnet top (CAT), lateral sides (CAS), and the upper part of the detector(CARD).

The electromagnetic imaging calorimeter comprises 44 single-sided silicon sensor planes, orthogonally arranged, interleaved with 22 plates of tungsten absorber. With a total depth of  $16.3\ X_0$  and 0.6 nuclear interaction lengths, combines the topological information of the two views with the energy released in the silicon ( $dE/dx$ ), achieving a proton rejection factor of at least  $10^5$  above 10 GeV while maintaining an electron selection efficiency of  $\sim 90\%$ .

The neutron detector consists of 36  $^3\text{He}$  counters, inserted into a polyethylene moderator. It helps in hadrons and leptons discrimination in the high energy events along with the shower tail catcher scintillator (S4), which is attached at the calorimeter bottom above the neutron detector. The latter is made of a plastic scintillator layer viewed by a total of six photomultipliers.

PAMELA overall size is about  $130\times 70\times 70\ \text{cm}^3$ , corresponding to a geometric factor

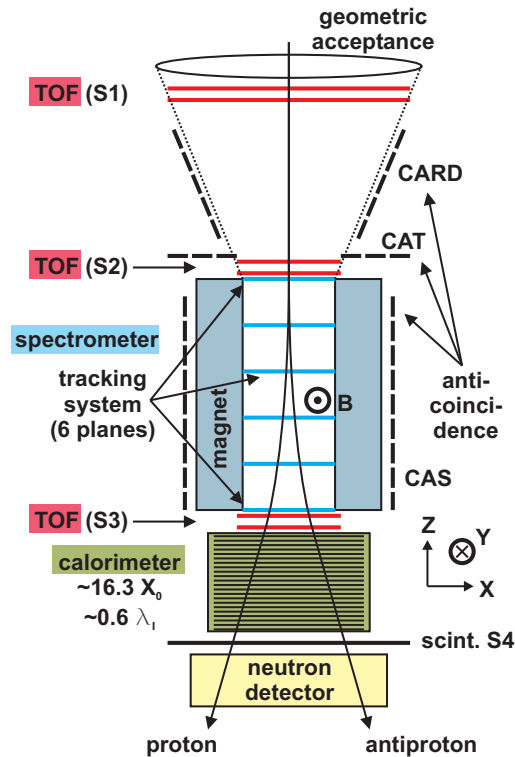


FIGURE 1. Sketch of the PAMELA apparatus.

of  $21.5 \text{ cm}^2\text{sr}$  ( for  $R > 1\text{GV}$ ), for a total mass of  $\sim 470 \text{ kg}$ , and a maximum power consumption of about  $360 \text{ W}$ .

## ANTIPROTON AND POSITRON SELECTION

Since the first days of operation, PAMELA, is transmitting to ground about  $16 \text{ GB}$  of data every day. After a quick look, to check the status of the detector, data are reduced and calibrated.

An event candidate, in PAMELA, is first checked for consistency in the rigidity determination procedure. Once a candidate track is selected then the particle type is identified using a combination of cut on several quantities calculated for each detector depending on the rigidity range and the nature of the particle to be identified.

Using the ToF, only down-going particles are selected. Then the charge sign is identified and the rigidity determined by the spectrometer using a recursive procedure. In this procedure the number of tracks cleanly entering the PAMELA acceptance, are de-

terminated and, for each track, also the quality of the track reconstruction along with the maximum detectable rigidity (MDR) achievable with the estimated track quality.

In selecting antiprotons the quality of the track information from the spectrometer is crucial. Due to the finite spectrometer resolution, corresponding in PAMELA to an MDR exceeding 1 TV, high rigidity protons may be assigned the wrong sign of curvature. In addition there is a background from protons which scatter in the material of the tracking system and mimic the trajectory of negatively-charged particles. These so called proton “spillover”, “spilling” from the positive to negative rigidity values, have to be eliminated in order to accurately determine the antiproton spectra. This was done by imposing a set of strict selection criteria on both the number of position measurements required on each view and a cut on the  $\chi^2$  obtained for the fitted track.

In Figure 2 is shown the deflection ( $1/\text{rigidity}$ ) distribution for proton (positively-charged) and antiproton (negatively-charged) candidates. The good separation between negatively-charge particles and spillover protons is evident, showing the effectiveness of the tracking requirements in limiting the spillover protons.

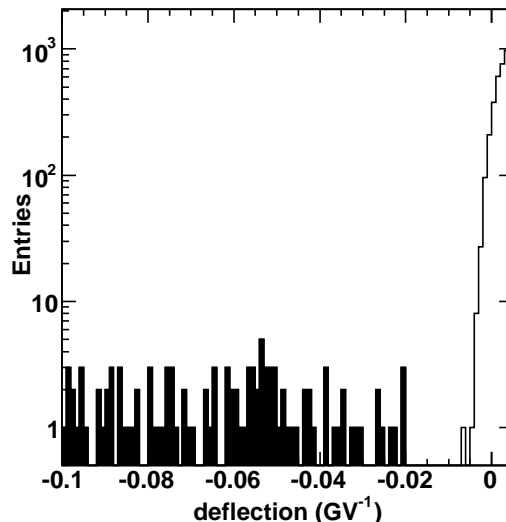


**FIGURE 2.** The deflection reconstructed by the track fitting procedure for proton (positive side, white filled histogram) and antiproton (negative side, black filled histogram) candidates.

The calorimeter is used to select events producing an electromagnetic shower, *i.e.* electrons and positrons. The longitudinal and transverse segmentation of the calorimeter combined with  $dE/dx$  measurements from the individual silicon strips allow electromagnetic showers to be identified with very high accuracy. In the antiproton analysis the calorimeter is used to reject electrons; an energy dependent calorimeter selection has been defined comparing electron data samples from simulations and particle beams, and antiproton data samples from simulations [3]. The deflection versus  $\beta$  of a smaller sample of antiproton and proton candidates is shown in Figure 3.

In case of positively-charged positrons spillover is due to negatively-charged electrons. After applying the set of strict selection criteria on the quality of the fitted tracks,

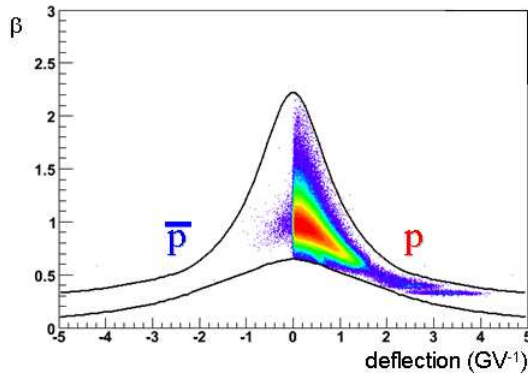


**FIGURE 3.** The deflection reconstructed by the track fitting procedure vs.  $\beta$  for proton (positive side) and antiproton (negative side) candidates. Full line correspond to the selection in  $\beta$ , red and blue colors corresponds to higher and lower counts respectively.

the spillover limit is estimated approximately at  $\sim 300$  GeV. This limit was estimated from flight data and simulation and checked using data from beam tests.

In the case of positron, calorimeter is used to positively identify events showing an electromagnetic cascade; at higher energy this signal is dominated by the proton background. The positron identification must be robust and the estimation of the residual proton background have to be accurate. From electron collected at test beam, we found that less than one proton out of 100,000 passes the calorimeter selection, identifying electromagnetic showers, for electrons up to 200 GeV/c, with a corresponding electron selection efficiency of 80%. However, for the positron analysis, a different approach is used: calorimeter identification was tuned to select  $>95\%$  of the electrons or positrons while rejecting 99.9% of the protons. After the selection the residual proton background was estimated using statistical methods.

One of the quantity used to identify an electromagnetic shower in the calorimeter is the fraction of energy deposited inside a cylinder of radius 0.3 Molière radii, as a function of deflection. The axis of the cylinder is defined by extrapolating the particle track reconstructed by the spectrometer. Event selection is further refined requiring a match between the momentum, as measured by the tracking system, and the total detected energy, as measured by the calorimeter. Besides the momentum–energy matching, a shower starting point selection criteria is applied requiring that the electromagnetic shower starts developing in the first planes of the calorimeter. In Figure 4, the distribution of the fraction of energy deposited along the track vs. deflection is shown for events passing the above mentioned selections. The red region indicate bins with larger number of events, clearly evidencing the electron and positron candidates.

Besides data collected in several test beam campaigns, a full detector simulation has been used to estimate or cross validate not only selection efficiencies and detector acceptance but also all possible backgrounds. The simulation is based on the GEANT3 [9] simulation package and fully describe the detector as well as his aluminum container. Simulation has been fine-tuned using the test beam data as well as data from the previ-

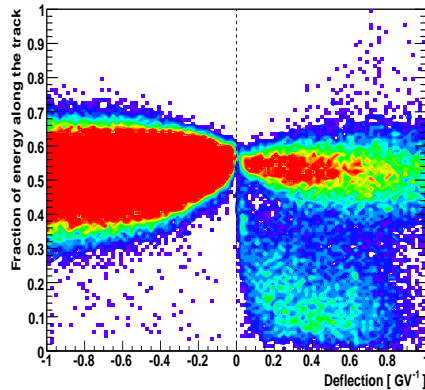


**FIGURE 4.** The fraction of energy deposited in the calorimeter along the track vs deflection reconstructed by the track fitting procedure. The red and blue colors corresponds to higher and lower counts respectively. electrons and positrons are comprised in the red areas.

ous ballon flights of the collaboration. Simulated data are digitized into an output format compatible with the PAMELA raw data format and analyzed using the full data reduction and offline analysis software used for the real data.

## BACKGROUNDS AND EFFICIENCIES ESTIMATION

The analysis of such rare components like antiprotons and positrons, needs a precise knowledge and understanding of all the possible sources of background. To estimate these we used more than one simulation packages, the test beam data and the flight data itself.

In the antiproton sample a possible contamination is due to negatively-charged pions produced by cosmic-ray interactions with the PAMELA payload and entering in the detector acceptance. Above  $1 \div 2$  GV  $\beta$  this is an irriducible background because measurements from the TOF are not sufficient to clearly discriminate pions from antiprotons. This background was studied using both simulated and flight data.

This secondary pion production from interaction of primaries in the upper part of the apparatus was simulated using both the GEANT3 full PAMELA simulation and a two step approach. In the latter the upper part of the detector is simulated using the FLUKA package[8] and, if a secondary particle is found in the spectrometer acceptance, the simulated event is passed to the full PAMELA simulation for propagation in the spectrometer and calorimeter and final data digitization. This two step approach better reproduced the pion spectra as found in the flight data, below 1 GV.

In the flight data, both negatively and positively-charged pions below 1 GV were identified using the  $\beta$  as measured by the ToF system combined with the calorimeter information, to reject electrons and positrons. The majority of these pion events had hits in the AC scintillators and/or large energy deposits in one of the top TOF scintillator pad-

dles, clearly indicating that they were the product of cosmic ray interactions with either the PAMELA structure or the pressure vessel. After applying all previously described selection criteria, the energy spectrum of the surviving pions was calculated below 1 GV and compared with the corresponding spectrum obtained from the simulation[4, 5]. After comparison with the experimental pion spectrum below 1 GV, a normalization factor, which accounted for all efficiencies not taken into account in the simulation, was obtained. The normalized simulated pion spectrum was used to estimate the contamination in the antiproton sample for rigidities greater than 1 GV. This procedure resulted in a residual pion contamination of less than 5% above 2 GV, decreasing to less than 1% above 5 GV. This result was cross-checked between 4 and 8 GV by selecting antiproton events below the geomagnetic cut-off. This sample includes re-entrant-albedo<sup>1</sup> antiprotons and locally produced pions. By scaling the number of such events for the acquisition time an upper limit for the negative pion (and protons with the wrong sign for the reconstructed deflection) contamination in the cosmic ray antiproton sample was found to be  $\sim 3\%$ , in agreement with simulations.

Also the resulting electron contamination, due to the calorimeter selection inefficiency, was estimated and found to be negligible across the whole energy range of interest.

Besides contamination, the efficiency for every detector were estimated. In particular the different, and momentum dependent, interaction cross sections for protons and antiprotons were taken into account in estimating the calorimeter selection efficiencies as a function of momentum for both species. These efficiencies were studied using both simulated antiprotons and protons samples along with proton selected from the flight data.

In the case of positron selection, it is mandatory to quantify the contamination due to protons missidentified as positron by the calorimeter. While in Figure 4 the distribution of the energy in the calorimeter shows a clear positron signature, the residual proton background distribution must be quantified. This distribution was obtained using the flight calorimeter data. The total calorimeter depth of 22 detector planes was divided in two non-mutually exclusive parts: an upper part comprising planes 1-20, and a lower part comprising planes 3-22. Calorimeter variables (e.g. total detected energy, and lateral shower spread) were evaluated for both parts. Electrons and positrons can be identified in the upper part of the calorimeter using the total detected energy and the starting point of the shower. A nearly pure sample of protons can be obtained in the lower part of the calorimeter (planes 3-22) selecting particles that do not interact in the first 2 planes (only 2% of electrons and positrons with rigidities greater than 1.5 GV pass this condition). This “pre-sample” procedure was validated using simulations and used to estimate the proton contamination in the positron sample. In Figure 5 the fraction of the energy deposited along the track for positron, electron and proton, selected using the “pre-sample” procedure, are shown.

A further validation of the calorimeter event selection methodology was done using

---

<sup>1</sup> Secondary particles produced by cosmic rays interacting with the Earth’s atmosphere that are scattered upward but lack sufficient energy to leave the Earth’s magnetic field and re-enter the atmosphere in the opposite hemisphere but at similar magnetic latitude.

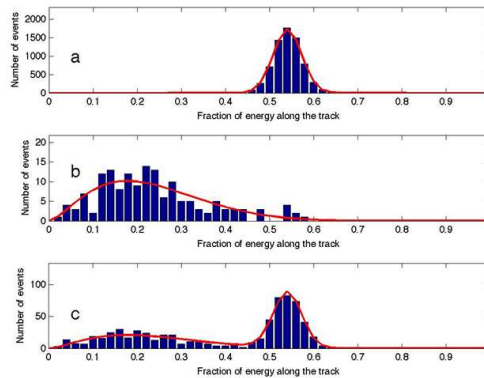


**FIGURE 5.** Fraction of energy along a track in the calorimeter in the “pre-sample” analysis. Panel a shows the distribution of the energy fraction for negatively charged particles with rigidity between 20 and 28 GV, selected as electrons in the upper part of the calorimeter. Panel b shows the same distribution for positively charged particles selected as protons in the bottom part of the calorimeter. Panel c shows positively charged particles, selected in the upper part of the calorimeter, i.e. protons and positrons.

the neutron yield from the calorimeter, as measured by the neutron detector, and the ionization ( $dE/dx$ ) losses as measured in the spectrometer. A higher neutron yield is expected in hadronic interactions in the calorimeter, especially at energies greater than 10 GeV. Similarly, competing density and logarithmic rise effects for  $dE/dx$  losses in the silicon detectors of the spectrometer should yield to different  $dE/dx$  distributions for electrons and protons between 10 and 25 GeV. These distributions were studied for positively and negatively-charged events after the calorimeter selection and compared to the corresponding distributions derived from the entire set of data for negatively charged, mostly electrons, and positively charged events, dominated by the protons. Also these checks confirmed the validity of the calorimeter selection criteria.

## CHARGE RATIO RESULTS

Once all the efficiencies and backgrounds have been estimated, fluxes of proton and antiproton, electron and positron have been calculated and charge ratios estimated. Results are showed in Fig. 6 and Fig. 7 where the antiproton to proton ratio is showed along with the one of the positron to the sum of the electron and positron. The antiproton selected candidates are slightly more than 1300, while the positron are more than 12000. For the first time these charge ratios have been investigated at energy larger than 50 GeV. Antiproton result are compatible with earlier data and do not show any clear deviation from a secondary production.

Positrons, instead, clearly show an excess at high energy; this can be due to dark matter particle annihilation in the galactic halo or to nearby sources, such as pulsar [7].

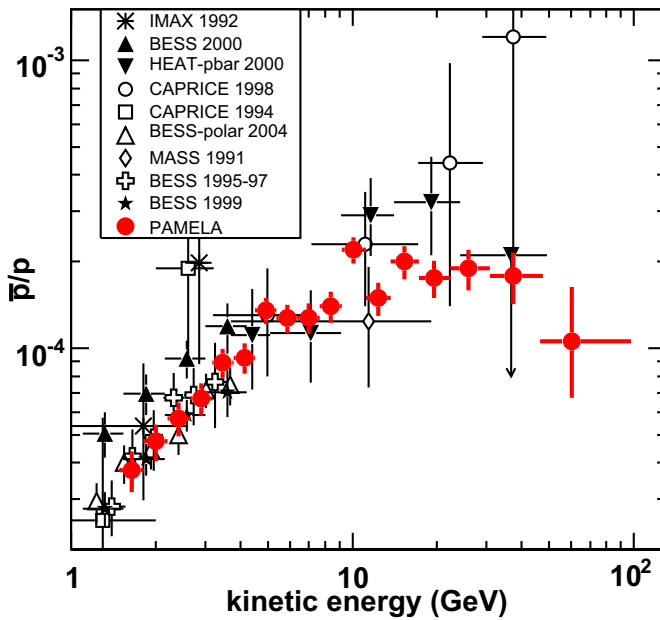


**FIGURE 6.** Antiproton to proton ratio between 1 and 100 GeV (left)[6]. The ratio is compared to recent measurements, see [6] for references

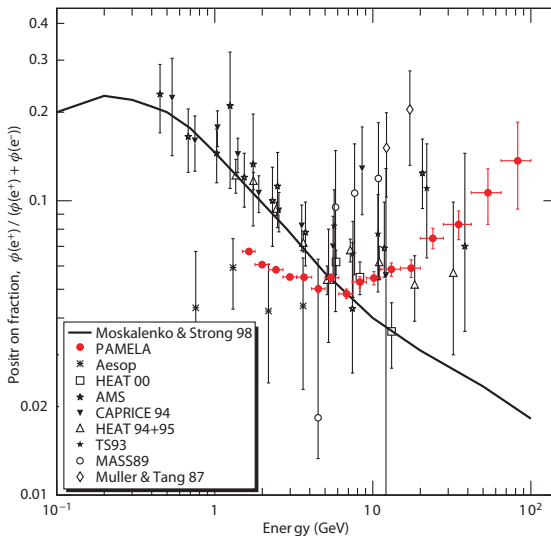


**FIGURE 7.** Positron to the sum of electron and positron ratio between 1.5 and 100 GeV (right)[7]. The ratio is compared to recent measurements, see [7] for references

## CONCLUSIONS

PAMELA is smoothly collecting data, recording the largest antiparticle statistic in the energy range up to 100 GeV.

For the first time the antiproton and positron charge ratios have been investigated at energy larger than 50 GeV. Antiproton result do not show any clear deviation from a secondary production. Positrons, instead, clearly show an excess at high energy.

These results have been extracted from the  $\sim 2 \times 10^9$  triggers that have been registered so far. Such a statistic allows for precise measurement of cosmic-ray spectra over a wide energy range, candidating PAMELA to be a permanent cosmic ray laboratory in space.

## REFERENCES

1. Picozza, P. *et al*, *Astropart. Phys.* **27**, 296–315 (2007).
2. Casolino, M. *et al*, *Two years of flight of the Pamela experiment: results and perspectives*, preprint at arXiv:0810.4980v1 [astro-ph].
3. Boezio, M. *et al*, *Astropart. Phys.* **26**, 111–118 (2006).
4. Hofverberg, P. , *Ph.D. thesis*, Royal Institute of Technology, Stockholm, 2008.
5. Bruno, A. , *Ph.D. thesis*, University of Bari, Bari, 2008.
6. Adriani, O. *et al*, *A new measurement of the antiproton-to-proton flux ratio up to 100 GeV in the cosmic radiation*, *Phys. Rev. Lett.* **102**, 051101, 2009 (arXiv:0810.4994v1 [astro-ph])
7. Adriani, O. *et al*, *Observation of an anomalous positron abundance in the cosmic radiation*, *Nature* **458**, 607–609, 2 April 2009 (arXiv: 0810.4995 [astro-ph])
8. A. Fassó, A. Ferrari, J. Ranft and P. R. Sala, *FLUKA: Status and Prospective for Hadronic Applications*, *Proc. of the MonteCarlo 2000 Conference*, Springer-Verlag, Berlin, 2001, pp. 955–960.
9. Brun, R. *et al*, *Detector Description and Simulation Tool*, CERN Program Library Long Writeup W5013. (1994).